Investigating the trade-off between color saturation and angle-independence in photonic glasses

Xiao, Ming; Stephenson, Anna B; Neophytou, Andreas; Hwang, Victoria; Chakrabarti, Dwaipayan; Manoharan, Vinothan N

DOI:
10.1364/OE.425399

Research Article | Vol. 29, No. 14 / 5 July 2021 / Optics Express 21212
Optics EXPRESS

Investigating the trade-off between color saturation and angle-independence in photonic glasses

MING XIAO,[1] ANNA B. STEPHENSON,[1] ANDREAS NEOPHYTOU,[2] VICTORIA HWANG,[1] DWAIPAYAN CHAKRABARTI,[2] AND VINOTHAN N. MANOHARAN[1,3,*]

[1]Harvard John A. Paulson School of Engineering and Applied Sciences, Harvard University, Cambridge, MA 02138, USA
[2]School of Chemistry, University of Birmingham, Birmingham B15 2TT, United Kingdom
[3]Department of Physics, Harvard University, Cambridge, MA 02138, USA
*vnm@seas.harvard.edu

Abstract: Photonic glasses—isotropic structures with short-range correlations—can produce structural colors with little angle-dependence, making them an alternative to dyes in applications such as cosmetics, coatings, and displays. However, the low angle-dependence is often accompanied by low color saturation. To investigate how the short-range correlations affect the trade-off between saturation and angle-independence, we vary the structure factor and use a Monte Carlo model of multiple scattering to investigate the resulting optical properties. We use structure factors derived from analytical models and calculated from simulations of disordered sphere packings. We show that the trade-off is controlled by the first peak of the structure factor. It is possible to break the trade-off by tuning the width of this peak and controlling the sample thickness. Practically, this result shows that the protocol used to pack particles into a photonic glass is important to the optical properties.

1. Introduction

Structural color results when specific wavelengths of light constructively interfere after scattering from a nanostructured material [1,2]. Conventional structural colors are produced by periodic nanostructures (photonic crystals) and are bright and highly angle-dependent [3]. However, some disordered structures with short-range correlations, called photonic glasses [4,5], can also produce structural colors [6–8]. These systems can be made by packing spherical colloidal nanoparticles. The colors of photonic glasses are less angle-dependent: the color does not vary with the orientation of the sample and varies much less than that of a photonic crystal with the angle between the light source and viewer. These features make these materials a promising alternative to dyes for wide-angle applications like cosmetics, displays, and coatings [9–11].

For these applications, high color saturation is required, but for most photonic glasses, the colors are not highly saturated. Thus, broadband absorbers like carbon black [12] and melanin [13,14] are often added to increase the saturation. Indeed, it is difficult to make photonic glasses with colors that are both highly saturated and angle-independent without absorption [15,16]. However, the physical origins of the trade-off between saturation and angle-independence have not been explored in detail. The main challenge is to account for multiple scattering, which is present in nearly all photonic glasses and can strongly affect the color saturation, as well as the angle-dependence [17].

Here we use a Monte Carlo simulation approach that explicitly models multiple scattering [18] to computationally explore how the short-range correlations affect both the angle-dependence and saturation of structural colors in the absence of absorption. In comparison to other numerical

#425399 https://doi.org/10.1364/OE.425399
Journal © 2021 Received 17 Mar 2021; revised 7 Jun 2021; accepted 8 Jun 2021; published 22 Jun 2021

Optics EXPRESS

models such as finite-difference time-domain (FDTD) simulations [15], the Monte Carlo model does not require a real-space structure, and it has a much lower computational cost, allowing us to explore many different variations of the structure. Unlike theoretical models based on the energy-density coherent-potential approximation [19,20], our model does not account for near-field effects, but such effects may not be relevant for structurally colored materials like those we investigate here [18].

Our approach takes advantage of the isotropy of photonic glasses, which allows us to express the degree of short-range order using the structure factor $S(q)$. For an isotropic system, $S(q)$ is a function of only the magnitude and not the direction of the scattering wavevector $\mathbf{q}$ [21]. With this simplification, we are able to efficiently simulate multiple scattering using a Monte Carlo approach [18]. We vary the degree of order through different models for the structure factor: (1) the Percus-Yevick model for a hard-sphere liquid [22–25]; (2) the Percus-Yevick structure factor with analytical modifications; and (3) packing simulations that allow direct calculation of the structure factor. We quantify the angle-dependence by measuring the variation of the reflectance spectrum with the incident angle. We show that the trade-off between color saturation and angle-independence in photonic glasses is controlled primarily by the first peak of the structure factor. We then show that it is possible to break the trade-off by tuning the width of this peak and controlling the sample thickness.

2. Methods

2.1. Multiple scattering model

We use a recently developed Monte Carlo multiple scattering model [18] to predict structural colors in disordered colloidal packings. In this model—inspired by previous work in physics [26] and ray-tracing methods in computer science [27,28]—we simulate how "packets" of photons propagate through a system of spherical colloidal particles, and we calculate the reflectance spectrum by counting how many packets exit into the backscattering hemisphere (Fig. 1(a)). The trajectories of the packets are determined by repeatedly sampling the angle of scattering from a phase function, which accounts for Mie scattering and for constructive interference described by a structure factor, and sampling the step length from an exponential distribution whose mean is the scattering length. We use an effective medium approximation when we calculate the phase function and scattering length, and we account for Fresnel reflections at the boundaries of the effective medium. The model is parameterized in terms of experimental quantities, including the refractive indices of matrix and particle, particle size, particle volume fraction, and sample thickness. It also takes as input a structure factor that characterizes the degree of order in the photonic glass. The study that introduced this approach [18] used the Percus-Yevick model to calculate the structure factor. The simulation results were in quantitative agreement with reflectance measurements of photonic glasses of varying thickness, volume fraction, and particle size. This agreement showed that the model captures the salient physical effects contributing to the color, including constructive interference, multiple scattering, and surface scattering. The details of the approximations used in the model and the computational approach are given in Ref. [18].

Here we use the model to quantify the angle-dependence of colloidal photonic glasses by simulating the reflectance spectra at different incident angles. Because the structures are isotropic, the colors are independent of the sample orientation, and therefore the reflection spectra depend only on the polar angle of incident light θ_{in} (Fig. 1(b)). We simulate light entering the sample at different polar angles and calculate the reflectance into the entire backscattering hemisphere. Because there are no approximations that break time-reversal symmetry, each of the light paths can be reversed. Thus, the resulting reflectance is equivalent to that obtained by illuminating the sample diffusely and measuring the reflectance at different viewing angles. These illumination and observation conditions mimic those relevant to applications such as paints and coatings.

Optics EXPRESS

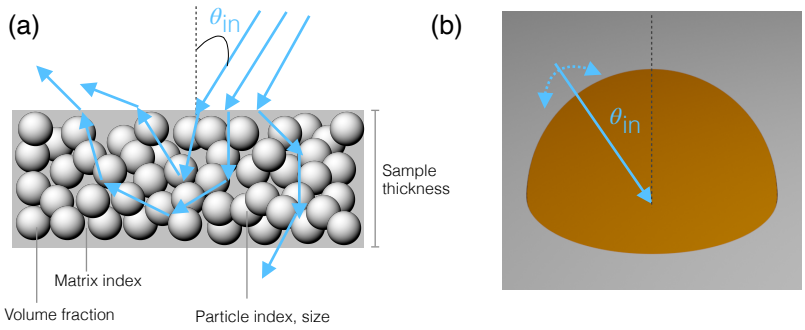

Fig. 1. Illustration of model and methods. (a) Diagram showing input parameters to the multiple scattering simulations. "Photon packets" (blue lines) enter the sample at an incident angle θ_{in}, scatter one or more times, then exit the sample. We calculate the reflectance spectrum by counting the percentage of trajectories that exit into the backscattering hemisphere. (b) Diagram showing the detector (brown) and incident light angle θ_{in}. To quantify the angle-dependence, we calculate the reflectance at the detector, which extends across the entire backscattering hemisphere, as a function of θ_{in}.

2.2. *Analytical structure factor calculation*

To calculate the structure factor analytically, we use the exact solution for $S(q)$ from Percus-Yevick theory [22], which describes the equilibrium thermodynamic properties of a fluid of hard spheres. The exact solution was obtained independently by Wertheim [23] and Thiele [24]. Ashcroft and Lekner [25] later expressed the solution for the structure factor as

$$S(qd) = 1/[1 - \rho c(qd)]\,, \tag{1}$$

where d is the particle diameter, ρ is the number density of spheres, and $c(qd)$ is the direct correlation function in momentum space,

$$c(qd) = -4\pi d^3 \int_0^1 s^2 \frac{\sin(sqd)}{sqd}\left(\alpha + \beta s + \gamma s^3\right) \mathrm{d}s, \tag{2}$$

where

$$\alpha = (1 + 2\phi)^2/(1 - \phi)^4\,, \tag{3}$$

$$\beta = -6\phi\,(1 + \phi/2)^2\,/(1 - \phi)^4\,, \tag{4}$$

$$\gamma = (1/2)\phi\,(1 + 2\phi)^2\,/(1 - \phi)^4\,, \tag{5}$$

and ϕ is the volume fraction of spheres. Ashcroft and Lekner [25] left the equation in these terms. We now integrate Eq. (2) and multiply by ρ to yield

$$\begin{aligned}\rho c(qd) = -\frac{24\phi}{(qd)^6}\Big\{&qd\sin(qd)\left[(qd)^2\,(\alpha + 2\beta + 4\gamma) - 24\gamma\right] - 2(qd)^2\beta \\ &- \cos(qd)\left[(qd)^4\,(\alpha + \beta + \gamma) - 2(qd)^2\,(\beta + 6\gamma) + 24\gamma\right] + 24\gamma\Big\}\,.\end{aligned} \tag{6}$$

As shown by Eqs. (6) and (1), the structure factor depends only on the volume fraction of particles and the dimensionless wavevector qd (Fig. 2(a)).

To gain a physical understanding of how the structure factor affects multiple scattering and the color, we analytically modify the peaks. To change the heights of the second and higher-order peaks relative to the first peak while keeping the first peak fixed, we start by locating the region

Optics EXPRESS

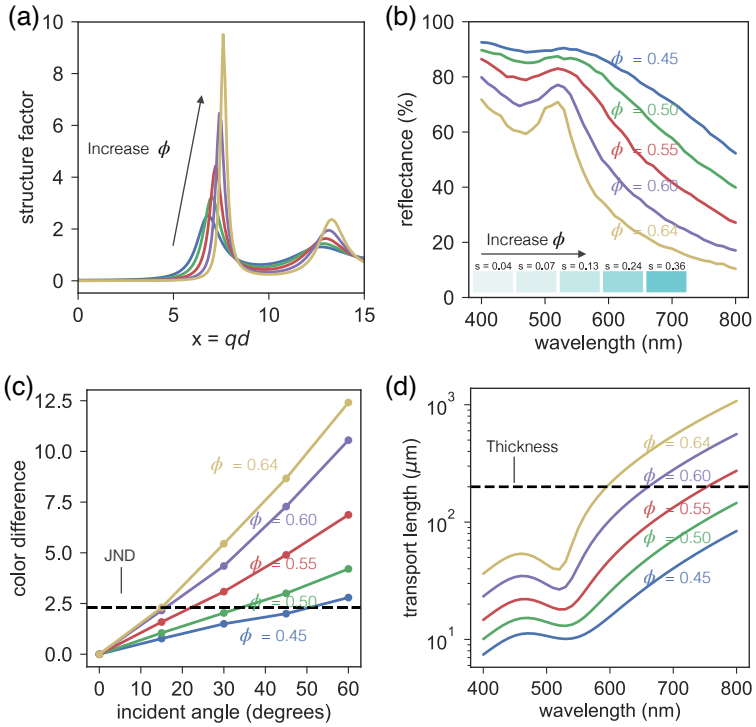

Fig. 2. Simulated optical properties of a silica-particle photonic glass, as calculated from our Monte Carlo model, using the Percus-Yevick structure factor at volume fractions of 0.45–0.64 (for other simulation parameters, see main text). (a) Structure factor at different volume fractions calculated using Eqs. (2) and (6). (b) Simulated reflectance spectra at normal incidence ($\theta_{in} = 0°$). Insets show color swatches and saturations calculated as $\sqrt{a^{*2} + b^{*2}}/L^*$, where L^*, a^*, and b^* are the CIELAB coordinates. Dashed line corresponds to the JND. (c) CIE 1976 color difference as a function of incident angle, relative to the color at normal incidence. (d) Transport lengths as a function of wavelength for different volume fractions. Dashed line marks the sample thickness in the simulations.

of the first peak by finding the third root x_3 of the equation $S(x) = 1$. We then modify only the second and higher-order peaks by adjusting the structure factor for $qd > x_3$:

$$S(qd)_{new} = \begin{cases} z\,[S(qd) - 1] + 1 & qd > x_3, \\ S(qd) & \text{otherwise}, \end{cases} \tag{7}$$

where z is a correction factor, and a larger z leads to higher peaks. For the Percus-Yevick structure factor [Eq. (6)] at $\phi = 0.55$, we find $x_3 = 11.8$ and we use three values $z = 0.5, 1, 2$.

To change the height or width of the first peak of the Percus-Yevick structure factor, we first find the points where $S(qd)$ has its first maximum ($qd = x_{max}$) and minimum ($qd = x_{min}$). Because the peak is asymmetric, we modify the two sides separately:

$$S(qd)_{new} = \begin{cases} f(qd)[S(qd) - S(qd = 2)] + S(qd = 2) & 2 < qd \le x_{max}, \\ f(qd)[S(qd) - S(x_{min})] + S(x_{min}) & x_{max} < qd < x_{min}, \end{cases} \tag{8}$$

where $f(qd)$ is the correction function. We do not modify $S(qd)$ in the region $0 < qd < 2$ (Fig. 2(a)). To adjust the peak height and keep the peak width (full width at half maximum) constant, we use

Optics EXPRESS

a linear correction function:

$$f(qd) = \begin{cases} z(qd-2)/(x_{\max}-2) & 2<qd \le x_{\max}, \\ z(x_{\min}-qd)/(x_{\min}-x_{\max}) & x_{\max}<qd<x_{\min}, \end{cases} \tag{9}$$

where z is a correction factor. We use $z = 0.6, 1.0, 1.5$ to modify the height of the first peak of the Percus-Yevick structure factor at $\phi = 0.55$ to generate the structure factors in Fig. S1a-b. To change the peak width and keep the height constant, we use a sinusoid as a correction function:

$$f(qd) = \begin{cases} (z-1)\sin[\pi(qd-2)/(x_{\max}-2)]+1 & 2<qd \le x_{\max}, \\ 0.6(z-1)\sin[\pi(qd-x_{\max})/(x_{\min}-x_{\max})]+1 & x_{\max}<qd<x_{\min}. \end{cases} \tag{10}$$

We use $z = 1, 0.5, -0.2$ to generate the structure factors in Fig. S1c-d.

2.3. Numerical structure factor calculations

Because analytical structure factors do not always accurately describe real packings of colloidal spheres, particularly at high volume fractions, we also simulate a system of colloidal spheres to directly generate packings and calculate their structure factors numerically. To this end, we perform Monte Carlo simulations of $N = 10^4$ nearly hard-sphere particles in a cubic box with periodic boundary conditions. These particles interact with each other *via* a modified pairwise Weeks-Chandler-Anderson (WCA) potential [29]. The effective potential between a pair of particles is

$$v(r_{jk}) = \begin{cases} 4\varepsilon\left[\left(\frac{\sigma}{r_{jk}}\right)^{200} - \left(\frac{\sigma}{r_{jk}}\right)^{100} + 0.25\right] & \text{if } r_{jk} \le 2^{1/100}\sigma \\ 0 & \text{otherwise,} \end{cases} \tag{11}$$

where ε and σ are the characteristic energy and length parameters, respectively, defining the corresponding units and r_{jk} is the center-to-center separation between particles j and k. We carry out the simulations at a volume fraction of $\phi = 0.6034$ and reduced temperature $T^* = k_B T/\varepsilon = 1$, where k_B is Boltzmann's constant. The simulation consists of 10^6 Monte Carlo cycles, where each Monte Carlo cycle involves N random displacements of individual particles, and is initiated from a randomly jammed packing (RJP) configuration, as reported in Ref. [30]. The potential energy is calculated using a spherical cutoff of 1.1σ, and a cell-list is used for efficiency [31]. We compute the static structure factor as

$$S(q) = \frac{1}{N}\left\langle \sum_j^N \sum_k^N \exp\left(-i\mathbf{q}\cdot\mathbf{r}_{jk}\right)\right\rangle, \tag{12}$$

where $\mathbf{r}_{jk}$ is the center-to-center separation vector between particles j and k, and $\mathbf{q}$ is the wavevector, the magnitude of which ranges from 0 to $2\pi/l$ (l being the edge length of the cubic box). Here we express the structure factor as a function of the magnitude of the wavevector, $q = |\mathbf{q}|$, as applicable for an isotropic system [21]. We take the average over five representative configurations of the system following equilibration. We also calculate the structure factor for the initial RJP configuration to compare to our calculation for the WCA packing.

2.4. Calculation of color saturation and color difference

We use the CIELAB (CIE 1976) color space to quantify how the colors of the photonic glasses would be perceived by humans in a standardized setting: a standard observer (CIE 1931 2°) and

Optics EXPRESS

a standard illuminant (Daylight, D65) [32]. We calculate three color values, L^*, a^*,and b^* from simulated reflectance spectra (see Supplement). The color saturation is then calculated as [32]

$$s = \sqrt{a^{*2} + b^{*2}}/L^*. \tag{13}$$

Because CIELAB is a perceptual color space, we can quantify how observers would perceive the angle-dependence by calculating the CIE 1976 color difference [32]:

$$\Delta = \sqrt{(L_1^* - L_0^*)^2 + (a_1^* - a_0^*)^2 + (b_1^* - b_0^*)^2}. \tag{14}$$

2.5. Calculation of transport length

We use a single-scattering model to calculate the transport length (or transport mean free path) [16,17]. The transport length is a function of asymmetry parameter g, scattering cross section σ_{sc}, and the number density of scatters ρ:

$$l^* = \frac{1}{\rho\sigma_{sc}(1-g)}, \tag{15}$$

where $g = <\cos\theta>$ and θ is the scattering angle. The scattering cross section is related to both the form factor F and structure factor S [16,33]:

$$\sigma_{sc} = \frac{1}{k^2}\int_0^{2kd} F(q, kd)S(qd)qd\,\mathrm{d}(qd), \tag{16}$$

where $k = 2\pi n_{eff}/\lambda$ is the wavevector, n_{eff} is the effective medium, and λ is the wavelength of light in vacuum. $q = 2k\sin(\theta/2)$ is the magnitude of the momentum-transfer vector (difference between scattered and incident wavevectors), and d is the particle diameter.

3. Results

We first examine the effect of volume fraction on saturation and angle-dependence in hard-sphere packings, which are described by the Percus-Yevick structure factor. These calculations establish a baseline for the optical properties. We use our Monte Carlo approach to simulate light propagating through packed spherical silica particles (constant refractive index of 1.45 and radius of 125 nm) in air (matrix index 1.0). We ignore dispersion and absorption because our goal is to understand the effects of the structural correlations only. We choose a sample thickness of 200 µm so that the system scatters strongly but not diffusely.

As we increase the volume fraction from 0.45 to 0.64, we find that the first peak in the structure factor becomes higher and sharper (Fig. 2(a) and Fig. S2). The peak in the reflectance spectrum at around 520 nm, which corresponds to the first peak in the structure factor, also becomes sharper at higher volume fractions. Furthermore, the reflected intensity decreases across the spectrum (Fig. 2(b)), indicating a reduction in multiple scattering, as we discuss below. As a result, the saturation of the colors increases from 0.04 to 0.36 with increasing volume fraction (Fig. 2(b), insets).

This higher saturation is accompanied by an increase in angle-dependence, as shown in Fig. 2(c). At low volume fractions, the variation of color with the incident angle may not be perceivable to the human eye: the calculated CIE 1976 color differences are comparable to or smaller than 2.3, the "just noticeable difference" or JND, at which 50 % of observers can distinguish two colors [34]. At higher volume fractions, the color difference increases more rapidly with angle, reaching 4–5 times the JND. This variation in color would be perceivable by nearly all observers (see all color swatches in Fig. S3). For applications such as displays, a smaller angle-dependence would be desirable, without compromising saturation.

Optics EXPRESS

To understand the changes in color shown in Fig. 2, we examine how the transport length changes with volume fraction. The transport length is the distance over which light loses memory of its initial direction because of multiple scattering. Smaller transport lengths generally correspond to lower saturation because light with wavelengths outside the reflectance peak can be scattered back to the viewer [17]. For the simulated system of Fig. 2, we find that the transport length at all wavelengths increases with volume fraction (Fig. 2(d)). Although the volume fraction can affect both the form factor (through the effective refractive index) and the structure factor, we find that the contribution from the structure factor dominates (Fig. S4). At higher volume fractions, the peak of the structure factor becomes sharper, leading to a larger transport length and a larger dip in the transport length at the corresponding reflectance peak. The larger transport length reduces the multiple scattering, while the dip in the transport length near the reflection peak results from increased backscattering due to constructive interference. The combination of the two effects leads to more saturated colors.

To gain physical insight into how the peaks in the structure factor affect the colors, we modify the Percus-Yevick structure factor analytically and simulate scattering from the resulting photonic glasses. Our modified structure factors do not necessarily correspond to real packings; instead, they serve only to help us understand how different types of spatial correlations affect the color saturation and angle dependence. We simulate scattering from packings with the modified structure factors at a constant volume fraction $\phi = 0.55$, which is below the maximum random packing density [35] and is readily approached in experiments [36].

We find that when we change the amplitudes of the second and higher-order peaks relative to the first, the reflectance spectrum and color saturation do not change (Fig. 3(a)-(b)), and the angle-dependence also remains the same (Fig. 3(c)). This result is not surprising, because changes in the structure factor at large q do not affect the scattering at visible wavelengths. These changes can in principle affect the scattering in the ultraviolet (UV) region (200 nm to 400 nm), and in other systems, the second peak in the structure factor and the dip between the first and second peaks can contribute to the reflectance spectrum at short wavelengths [16]. Here, however, the first peak alone controls both the reflectance spectrum and the angle-dependence, even in the UV.

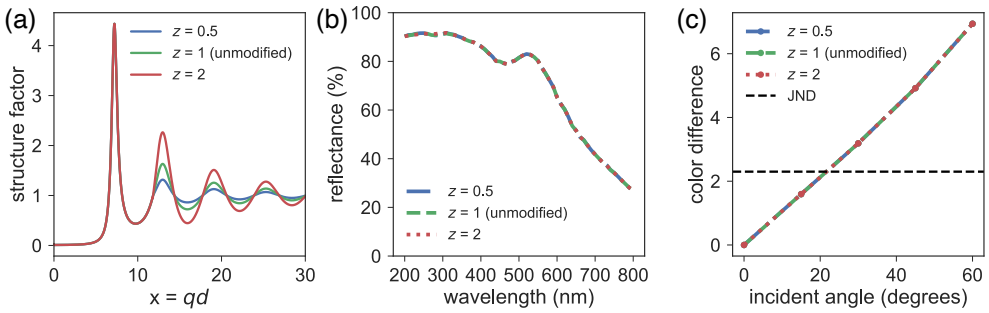

Fig. 3. The effects of the second and higher-order peaks of the Percus-Yevick structure factor on the reflection spectra for the simulated silica system described in the main text. (a) Plots of Percus-Yevick structure factors, modified so that the amplitude of the first peak is constant and the amplitudes of the higher-order peaks are changed. (b) Simulated reflectance spectra at normal incidence for the three structure factors in (a). (c) Color variation with incident angle, as quantified by CIE 1976 color difference from normal incidence.

Although we can intuitively deduce from Eq. (16) how the structure factor affects properties such as the reflection peak sharpness, the saturation and angle-dependence must be calculated from our model because they are affected by multiple scattering. To understand how the

Optics EXPRESS

correlations in the photonic glass affect these properties, we examine the effects of changing the height and width of the first peak independently.

We find that as the height increases and the width remains the same, the reflectance increases and the width of the reflectance peak slightly decreases. The resulting colors are less saturated and less angle-dependent (Fig. 4(a)-(c)). As the width decreases and the height remains the same, the reflectance decreases, and the colors are more saturated and more angle-dependent (Fig. 4(d)-(f)). We see a similar trend for blue and purple colors, which we simulate by using other particle sizes (Figs. S5 and S6). Thus, changing only the height or width of the first peak does not break the trade-off between saturation and angle-independence.

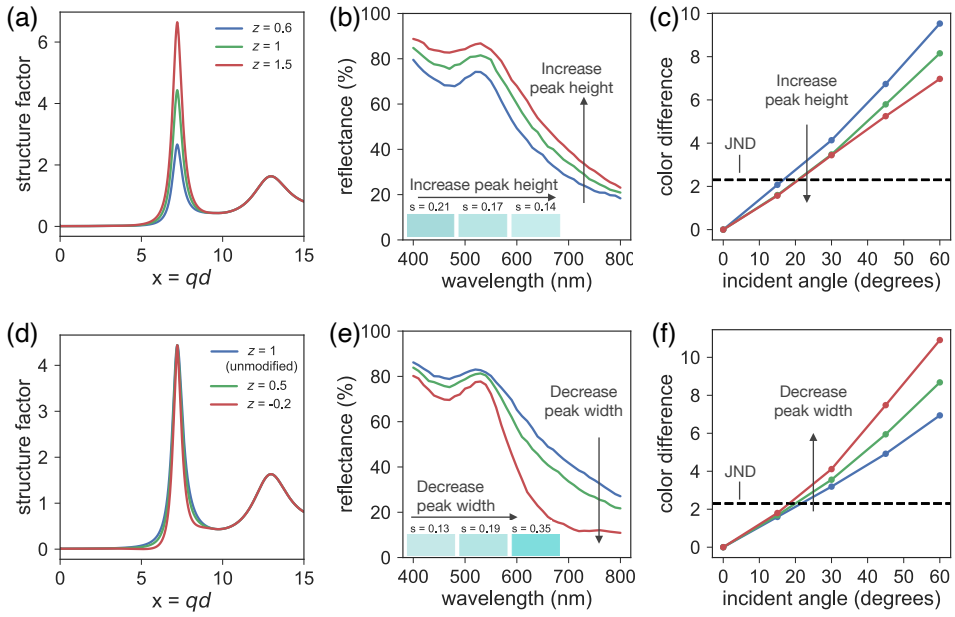

Fig. 4. The effects of changing the height or width of the first peak of the Percus-Yevick structure factor on the reflectance spectra for the simulated silica system. See Sec. 2.2 and Fig. S1 for details on how we modify the structure factor. (a) Plots of Percus-Yevick structure factors, modified so that the height of the first peak changes while the width remains constant. (b) Resulting simulated reflectance spectrum with $\theta_{in} = 0^{\circ}$ and (c) color variation with incident angle. Line colors (red, green, blue) correspond to the structure factors shown in (a). (d-f) Same as for (a-c), but with structure factors modified so that the width of the first peak decreases while the height remains the same. Insets in (b, e) are color swatches generated from the simulated spectra, along with saturation values.

To make sense of these results, we examine how the transport length changes as we modify the first peak of the structure factor. We find that decreasing either the height or width increases the magnitude of the transport length across the visible range (Fig. 5). This increase in transport length results in less multiple scattering and thus more saturated colors. Interestingly, reducing the peak width increases the transport length at long wavelengths much more than at shorter wavelengths, which would result in much less long-wavelength background scattering. This result explains why the most saturated colors shown in Fig. 4 are obtained by decreasing the peak width.

Because changing the peak height appears to simply rescale the transport length relative to the sample thickness (Fig. 5(a)), we examine the effect of changing the sample thickness. We find that when we set the thickness to the average transport length (averaged over the 400 nm to 800 nm

Optics EXPRESS

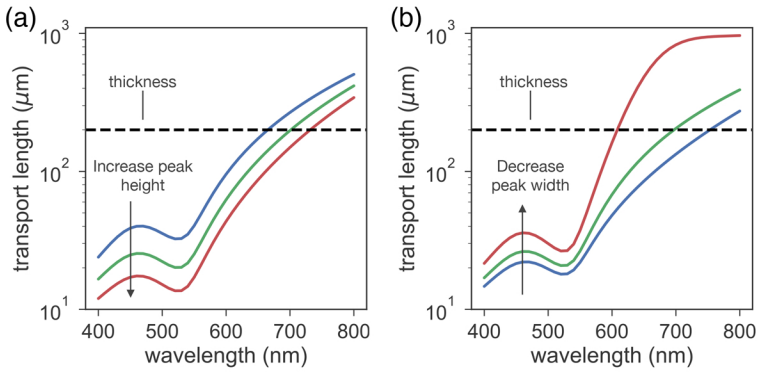

Fig. 5. Transport length as a function of wavelength for the simulated silica system. (a) Effects of changing the peak height of the Percus-Yevick structure factor while keeping the width constant. (b) Effects of changing the peak width while keeping the height constant. The corresponding structure factors are shown in Fig. 4(a) and Fig. 4(d). The dashed line represents the sample thickness.

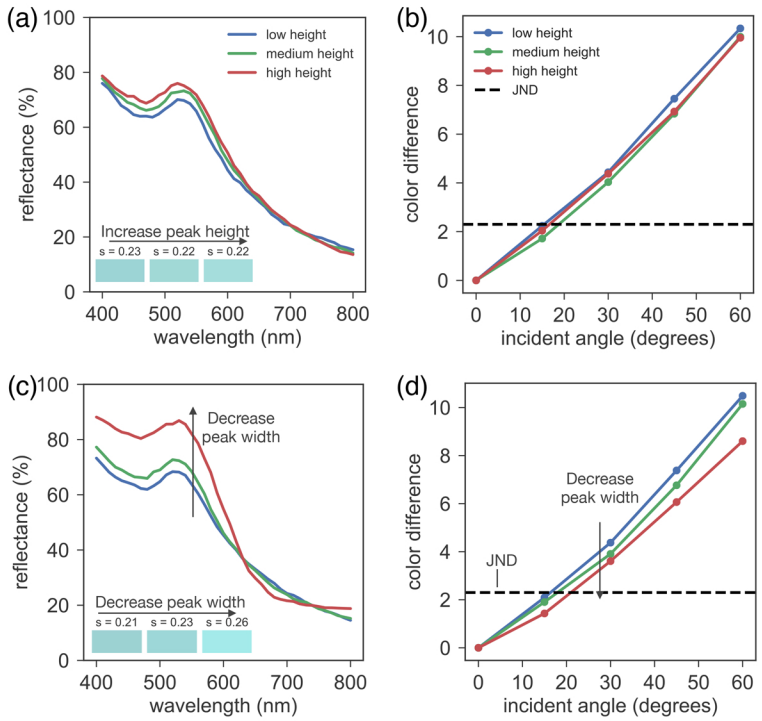

Fig. 6. Reflectance spectra, color saturation, and angle-dependence for the silica system, simulated using modified Percus-Yevick structure factors and with sample thicknesses set to the average transport length from 400 nm to 800 nm. (a) Reflectance spectra with $\theta_{in} = 0^{\circ}$ and (b) variation of color with incident angle for the structure factors shown in Fig. 4(a). The sample thicknesses are 162.9 μm (blue curve), 121.9 μm (green curve), and 93.4 μm (red curve). (c-d) As in (a-b), but for the structure factors shown in Fig. 4(d). The sample thicknesses are 84.3 μm (blue curve), 122.6 μm (green curve), and 379.1 μm (red curve).

Optics EXPRESS

range) at each peak height, the reflectance spectrum, color saturation, and angle-dependence do not change significantly (Fig. 6(a)-(b)). At long wavelengths, far from the reflection peak, the reflectance is about 20 %, higher than the amount expected from Fresnel reflections. This background reflectance comes primarily from low-order multiple scattering, which can occur even when the thickness of the sample is smaller than the transport length. Overall, the results show that increasing the height of the first peak of the structure factor at constant width has nearly the same effect as changing the sample thickness.

By contrast, decreasing the peak width while setting the sample thickness to the average transport length produces colors with higher saturation and *lower* angle-dependence (Fig. 6(c)-d). Thus, decreasing the width does not simply rescale the transport length; it also changes the shape of the plot of transport length as a function of wavelength. Here we choose to set the thickness to the average transport length because this choice makes the thickness greater than the transport length at shorter wavelengths, where the peak is located. As a result, multiple scattering near the peak increases, which has been shown to increase color saturation [17]. The accompanying reduction in angle-dependence that we observe suggests that we can break the trade-off between color saturation and angle-dependence by decreasing the width of the first peak of the structure factor while controlling the sample thickness.

With this understanding, we examine whether it is possible to break the trade-off in a real colloidal system. To this end, we numerically generate spherical packings with different structure factors at the same volume fraction, and we simulate their optical properties. We generate the

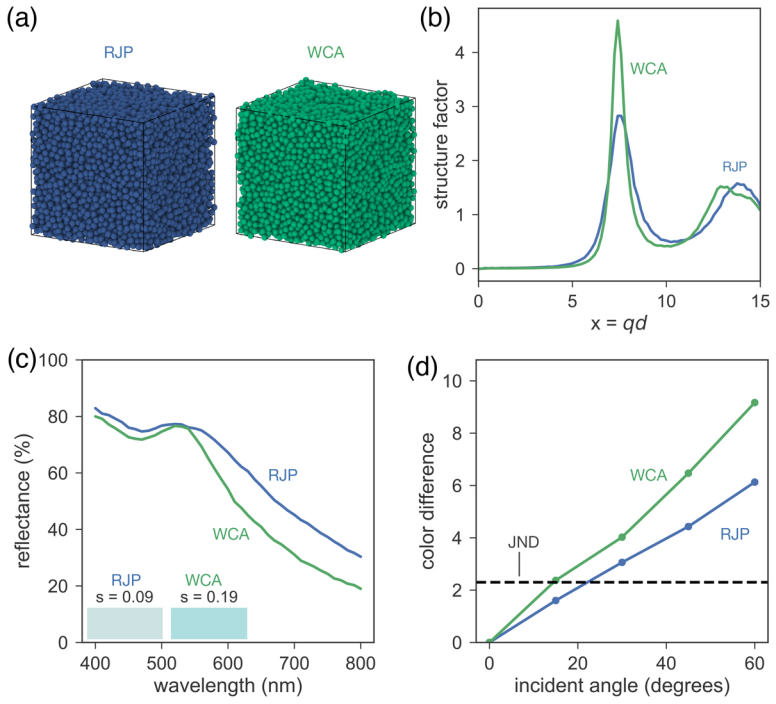

Fig. 7. Effects of changing the structure factor in more realistic packing of colloidal particles. (a) Renderings of the real-space structures of the simulated RJP and WCA packings. (b) Structure factor calculated from the simulated packings. (c) Simulated reflectance spectra for the two packings with $\theta_{in} = 0°$. Insets show color swatches and saturation values. (d) Color variation as a function of incident angle. The sample thickness is 200 µm in both cases.

Optics EXPRESS

packings by starting from a randomly jammed packing (RJP) simulated by Song and coworkers [30], introducing a Weeks-Chandler-Anderson (WCA) potential, and equilibrating the structure through a Monte Carlo algorithm (see details in Sec. 2.3). We choose $\phi = 0.6034$ for both packings to obtain structure factors that are different for the two packings. Snapshots of the initial (RJP) and equilibrated (WCA) structures are shown in Fig. 7(a). Compared to the RJP packing, the WCA packing has a higher and narrower first peak (Fig. 7(b)), showing that WCA has a higher degree of positional correlation. There is also a small shift in the peak of the structure factor, indicating that the average interparticle distance is different in the two packings.

The increase in peak height and the decrease in width from RJP to WCA have conflicting optical effects: the higher peak height should lead to less saturated color and lower angle-dependence, while the decrease in width should lead to more saturated color and higher angle-dependence. We find that the color of the WCA packing is more saturated and more angle-dependent than that of the RJP packing (Fig. 7(c)-(d)), suggesting that the peak width has a larger effect than the peak height does. However, if we set the sample thickness equal to the average transport length (Fig. 8(a)) in each packing, we find that the WCA packing has a more saturated color than the RJP but with a similar angle-dependence (Fig. 8(b)-(c)). This result shows that it is indeed possible to break the trade-off in a realistic system.

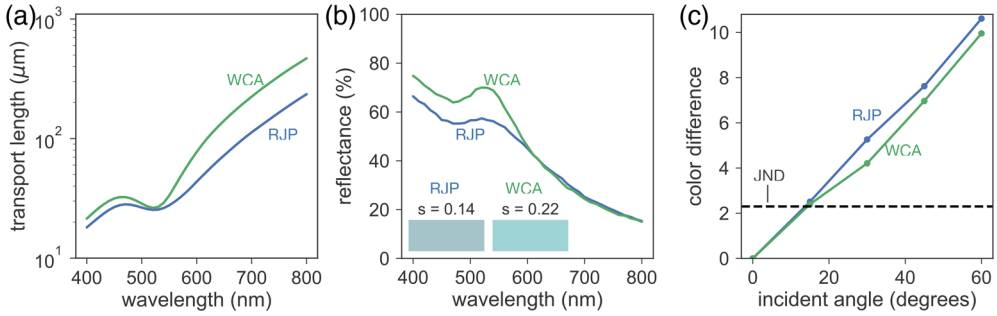

Fig. 8. Optical properties of RJP and WCA packings with sample thickness set to the average transport length in each case. (a) Transport length as a function of wavelength for the two packings. (b) Simulated reflectance spectra with $\theta_{in} = 0°$. Insets show color swatches and saturation values. (c) Color variation with incident angle. The sample thicknesses are 75.8 μm for the RJP packing and 140.6 μm for the WCA packing.

4. Discussion and conclusion

Our simulation results show that there is a trade-off between color saturation and angle-independence in photonic glasses that is controlled by the shape of the first peak of the structure factor. Whereas the height of the peak appears to simply rescale the transport length, the width of the peak changes the shape of the transport length as a function of wavelength. Systems with a narrow first peak have a much larger transport length at long wavelengths, which reduces multiple scattering and increases color saturation. One can use this effect to break the trade-off between color saturation and angle-independence. To do this, one must control both the width of the first peak of the structure factor and the thickness of the sample.

While it is straightforward to control the sample thickness experimentally [12,17,37], it is more challenging to control the width of the first peak. Our packing simulations show that it should be possible to vary the peak width by changing the packing protocol. Some protocols—slip-casting or rapid centrifugation [16,38], for example—are likely to lead to RJP-like structures, whereas others—centrifugation followed by equilibration in a liquid, for example—might lead to structures

Optics EXPRESS

more like our WCA packings, where the number of touching particles is smaller than in RJP. Other experimental approaches, such as changing salt concentration [39], using binary particles [12], and using an electric field [40], can also be used to change the packing. Therefore the width of the structure factor *can* be varied experimentally, though it is not yet clear how to optimize the packing protocol or synthesis to obtain a desired combination of saturation and angle-independence. Nor is it yet clear what fundamental or practical limits there are to achieving both high color saturation and low angle-dependence. Future studies might examine these topics, along with the question of how absorption affects the trade-off between color saturation and angle-independence. The primary conclusion from the current study is that it is possible—at least to some extent—to break the trade-off in photonic glasses through the packing protocol. This result can be used to guide the design of materials with prescribed color effects.

Funding. BASF Corporation; National Science Foundation (DGE-1144152, DMR-2011754); Institute of Advanced Studies, University of Birmingham.

Acknowledgments. We thank Rupa Darji, Keith Task, Mark Schroeder, Bernhard von Vacano, Rupert Konradi, Brian Leahy, Ahmed Sherif, Jennifer McGuire, and Caroline Martin for discussions on the manuscript.

Disclosures. MX, ABS, VH, VNM: BASF Corporation (F, P).

Data availability. Data from the optical and packing simulations shown in this paper are available in Ref. [41]. Source code for the optical simulations is available in Ref. [42].

Supplemental document. See Supplement 1 for supporting content.

References

1. S. Kinoshita, *Structural Colors in the Realm of Nature* (World Scientific, 2008).
2. V. E. Johansen, O. D. Onelli, L. M. Steiner, and S. Vignolini, "Photonics in nature: from order to disorder," in *Functional Surfaces in Biology III: Diversity of the Physical Phenomena*, S. N. Gorb and E. V. Gorb, eds. (Springer, 2017), pp. 53–89.
3. J. D. Joannopoulos, S. G. Johnson, J. N. Winn, and R. D. Meade, *Molding the Flow of Light* (Princeton University, 2008).
4. J. Ballato, "Tailoring visible photonic bandgaps through microstructural order and coupled material effects in SiO2 colloidal crystals," J. Opt. Soc. Am. B **17**(2), 219–225 (2000).
5. P. D. García, R. Sapienza, Á. Blanco, and C. López, "Photonic glass: A novel random material for light," Adv. Mater. **19**(18), 2597–2602 (2007).
6. L. Schertel, L. Siedentop, J.-M. Meijer, P. Keim, C. M. Aegerter, G. J. Aubry, and G. Maret, "The structural colors of photonic glasses," Adv. Opt. Mater. **7**(15), 1900442 (2019).
7. G. Shang, Y. Häntsch, K. P. Furlan, R. Janßen, G. A. Schneider, A. Petrov, and M. Eich, "Highly selective photonic glass filter for saturated blue structural color," APL Photonics **4**(4), 046101 (2019).
8. G. Shang, K. P. Furlan, R. Janßen, A. Petrov, and M. Eich, "Surface templated inverse photonic glass for saturated blue structural color," Opt. Express **28**(6), 7759 (2020).
9. D. Ge, E. Lee, L. Yang, Y. Cho, M. Li, D. S. Gianola, and S. Yang, "A robust smart window: reversibly switching from high transparency to angle-independent structural color display," Adv. Mater. **27**(15), 2489–2495 (2015).
10. Y. Ohtsuka, T. Seki, and Y. Takeoka, "Thermally tunable hydrogels displaying angle-independent structural colors," Angew. Chem. Int. Ed. **54**(51), 15368–15373 (2015).
11. H. Tan, Q. Lyu, Z. Xie, M. Li, K. Wang, K. Wang, B. Xiong, L. Zhang, and J. Zhu, "Metallosupramolecular photonic elastomers with self-healing capability and angle-independent color," Adv. Mater. **31**(6), 1805496 (2018).
12. J. D. Forster, H. Noh, S. F. Liew, V. Saranathan, C. F. Schreck, L. Yang, J.-G. Park, R. O. Prum, S. G. J. Mochrie, C. S. O'Hern, H. Cao, and E. R. Dufresne, "Biomimetic isotropic nanostructures for structural coloration," Adv. Mater. **22**(26-27), 2939–2944 (2010).
13. M. Xiao, Z. Hu, Z. Wang, Y. Li, A. D. Tormo, N. L. Thomas, B. Wang, N. C. Gianneschi, M. D. Shawkey, and A. Dhinojwala, "Bioinspired bright noniridescent photonic melanin supraballs," Sci. Adv. **3**(9), e1701151 (2017).
14. Y. Zhang, B. Dong, A. Chen, X. Liu, L. Shi, and J. Zi, "Using cuttlefish ink as an additive to produce non-iridescent structural colors of high color visibility," Adv. Mater. **27**(32), 4719–4724 (2015).
15. G. Jacucci, S. Vignolini, and L. Schertel, "The limitations of extending nature's color palette in correlated, disordered systems," Proc. Natl. Acad. Sci. **117**(38), 23345–23349 (2020).
16. S. Magkiriadou, J.-G. Park, Y.-S. Kim, and V. N. Manoharan, "Absence of red structural color in photonic glasses, bird feathers, and certain beetles," Phys. Rev. E **90**(6), 062302 (2014).
17. V. Hwang, A. B. Stephenson, S. Magkiriadou, J.-G. Park, and V. N. Manoharan, "Effects of multiple scattering on angle-independent structural color in disordered colloidal materials," Phys. Rev. E **101**(1), 012614 (2020).

Optics EXPRESS

18. V. Hwang, A. B. Stephenson, S. Barkley, S. Brandt, M. Xiao, J. Aizenberg, and V. N. Manoharan, "Designing angle-independent structural colors using Monte Carlo simulations of multiple scattering," Proc. Natl. Acad. Sci. **118**(4), e2015551118 (2021).
19. L. Maiwald, S. Lang, D. Jalas, H. Renner, A. Y. Petrov, and M. Eich, "Ewald sphere construction for structural colors," Opt. Express **26**(9), 11352–11365 (2018).
20. G. J. Aubry, L. Schertel, M. Chen, H. Weyer, C. M. Aegerter, S. Polarz, H. Cölfen, and G. Maret, "Resonant transport and near-field effects in photonic glasses," Phys. Rev. A **96**(4), 043871 (2017).
21. P. M. Chaikin, T. C. Lubensky, and T. A. Witten, *Principles of Condensed Matter Physics* (Cambridge University, 1995).
22. J. K. Percus and G. J. Yevick, "Analysis of classical statistical mechanics by means of collective coordinates," Phys. Rev. **110**(1), 1–13 (1958).
23. M. S. Wertheim, "Exact solution of the Percus-Yevick integral equation for hard spheres," Phys. Rev. Lett. **10**(8), 321–323 (1963).
24. E. Thiele, "Equation of state for hard spheres," J. Chem. Phys. **39**(2), 474–479 (1963).
25. N. W. Ashcroft and J. Lekner, "Structure and resistivity of liquid metals," Phys. Rev. **145**(1), 83–90 (1966).
26. L. Wang, S. L. Jacques, and L. Zheng, "MCML–Monte Carlo modeling of light transport in multi-layered tissues," Comput. Methods Programs Biomed. **47**(2), 131–146 (1995).
27. J. R. Frisvad, N. J. Christensen, and H. W. Jensen, "Computing the scattering properties of participating media using Lorenz-Mie theory," ACM Trans. Graph. **26**(3), 60 (2007).
28. I. Gkioulekas, B. Xiao, S. Zhao, E. H. Adelson, T. Zickler, and K. Bala, "Understanding the role of phase function in translucent appearance," ACM Trans. Graph. **32**(5), 1–19 (2013).
29. J. D. Weeks, D. Chandler, and H. C. Andersen, "Role of repulsive forces in determining the equilibrium structure of simple liquids," J. Chem. Phys. **54**(12), 5237–5247 (1971).
30. C. Song, P. Wang, and H. A. Makse, "A phase diagram for jammed matter," Nature **453**(7195), 629–632 (2008).
31. D. Frenkel and B. Smit, *Understanding Molecular Simulation: From Algorithms to Applications*, vol. 1 of *Computational Science Series* (Academic, 2001), 2nd ed.
32. G. A. Klein and T. Meyrath, *Industrial Color Physics* (Springer, 2010).
33. P. D. Kaplan, A. D. Dinsmore, A. G. Yodh, and D. J. Pine, "Diffuse-transmission spectroscopy: A structural probe of opaque colloidal mixtures," Phys. Rev. E **50**(6), 4827–4835 (1994).
34. G. Sharma and R. Bala, *Digital Color Imaging Handbook* (CRC, 2017).
35. S. Torquato, T. M. Truskett, and P. G. Debenedetti, "Is random close packing of spheres well defined?" Phys. Rev. Lett. **84**(10), 2064–2067 (2000).
36. M. Xiao, Y. Li, M. C. Allen, D. D. Deheyn, X. Yue, J. Zhao, N. C. Gianneschi, M. D. Shawkey, and A. Dhinojwala, "Bio-inspired structural colors produced via self-assembly of synthetic melanin nanoparticles," ACS Nano **9**(5), 5454–5460 (2015).
37. T. Liu, B. VanSaders, S. C. Glotzer, and M. J. Solomon, "Effect of defective microstructure and film thickness on the reflective structural color of self-assembled colloidal crystals," ACS Appl. Mater. Interfaces **12**(8), 9842–9850 (2020).
38. M. Reufer, L. F. Rojas-Ochoa, S. Eiden, J. J. Sáenz, and F. Scheffold, "Transport of light in amorphous photonic materials," Appl. Phys. Lett. **91**(17), 171904 (2007).
39. P. D. García, R. Sapienza, and C. López, "Photonic glasses: a step beyond white paint," Adv. Mater. **22**(1), 12–19 (2010).
40. I. Lee, D. Kim, J. Kal, H. Baek, D. Kwak, D. Go, E. Kim, C. Kang, J. Chung, Y. Jang, S. Ji, J. Joo, and Y. Kang, "Quasi-amorphous colloidal structures for electrically tunable full-color photonic pixels with angle-independency," Adv. Mater. **22**(44), 4973–4977 (2010).
41. M. Xiao, A. B. Stephenson, A. Neophytou, V. Hwang, D. Chakrabarti, and V. N. Manoharan, "Data for 'Investigating the trade-off between color saturation and angle-independence in photonic glasses'," https://doi.org/10.7910/DVN/DXKDBS, Harvard Dataverse, V2 (2021).
42. S. Magkiriadou, V. Hwang, A. B. Stephenson, S. Barkley, and V. N. Manoharan, "`structural-color` - A Python package for modeling angle-independent structural color," (2020). The source package can be found at https://github.com/manoharan-lab/structural-color.